PAPER

Check for updates

Synthesis of a high-silica intersecting-large-pore zeolite using hydrogen-bond-assisted structure-directing agents

Hao Li, Zhenghan Zhang, Yanan Xu, Shiyue Zhang, Pengliang Gu, Qing Hu, Yu Zhang, Wenkai Wang, Zhan Shi, Xinyi Fu, Jian Li* and Hongbin Du [ID] *

The targeted synthesis of silicate zeolites with specific pore structures has been one of the great challenges for synthetic chemists. Herein, we report a new zeolite synthesis strategy for the preparation of high-silica and all-silica large-pore zeolites by utilizing hydroxyl-containing organic cations as structure-directing agents. These cations form hydrogen-bonding assemblies during the low-temperature aging stage, thereby directing the formation of the high-silica and all-silica zeolite NUD-19. NUD-19 is topologically related to the germanosilicates ITQ-21 and NUD-3, and is topologically identical to germanate PKU-14, possessing a three-dimensional intersecting 12-membered-ring large-pore network with spherical 1.18 nm-diameter cavities. NUD-19 remains structurally stable after calcination at 550 °C and displays permanent porosity with micropores, mesopores, and macropores, making it a promising candidate for application in the fields of catalysis, adsorption, and separation. This preparative method could be applied to synthesize large-pore and ultra-large-pore zeolites that are not readily obtained under conventional conditions.

1. Introduction

Zeolites have attracted much attention because of their wide range of industrial applications in catalysis, adsorption, and separation.[1–3] Since the properties of zeolites are heavily influenced by their structure, efforts have been devoted to the preparation of zeolites with new framework types and structures.[4,5] To date, 258 zeolite frameworks have been named by the International Zeolite Association Structures Committee.[6] These include seventeen interrupted structures with triple-connected tetrahedra, whose novel porous structure may offer interesting properties, such as better selectivity between adsorbed molecules and framework defects.[7] Most of the Si-OH hydroxyl termini in these zeolites point to the channel.[8–10] When the four terminal oxygen atoms are located around a space similar to that occupied by a single Si atom, it can be regarded as a Si vacancy, and this unique structural feature may endow the zeolite with better selectivity and catalytic properties, *e.g.*, –SVR[11] and IDM-1.[12] Therefore, these kinds of zeolites with ordered vacancies have attracted great interest.

ITQ-21 is a germanosilicate zeolite with a three-dimensional pore network containing spherical 1.18 nm-diameter cavities formed by the intersection of three perpendicular linear 12-member-ring (12R) channels, which resembles that of zeolite Y or faujasite and shows promise for catalytic cracking applications.[13] The structure of ITQ-21 is closely related to those of two other materials, germanate PKU-14[14] and germanosilicate NUD-3.[15] The three zeolites possess an identical pore network, formed by connecting $[4^6 6^{12}]$ cage units. However, inside the cage unit, ITQ-21 and NUD-3 have a disordered and an ordered four-membered ring (4R), respectively, while PKU-14 lacks the four-membered ring inside the cage, enclosing an empty void of 4.2 Å in diameter. The defective structure of PKU-14 likely results in interesting, unique catalytic sites different to those of ITQ-21 and NUD-3. Unfortunately, the reported PKU-14 belongs to the pure germanate zeolite family, which is not stable and decomposes at 350 °C.[14] The synthesis of stable, high-silica form of PKU-14 is of significance in research yet a challenging task.

Structure-directing methods have been widely used in the crystallization of zeolites. The greater the interactions between a structure-directing agent (SDA) and a zeolite of specific structure, the greater the likelihood of success in forming that zeolite. Therefore, many efforts have been made in zeolite synthesis using organic cations of varied size, shape and hydrophilicity as SDAs.[16] This strategy has been successfully used in the synthesis of various zeolites with novel topology and

State Key Laboratory of Coordination Chemistry, School of Chemistry and Chemical Engineering, Nanjing University, Nanjing, 210023, China. E-mail: jian.li@nju.edu.cn, hbdu@nju.edu.cn

composition.[17–19] For the preparation of large-pore and extra-large-pore zeolites, obtaining large organic cations with suitable hydrophilicity is often challenging. However, aromatic organic cations have been found to form larger supramolecular assemblies through interactions between the aromatic rings, which effectively function as SDAs for the formation of large- and extra-large-pore zeolites.[20–22]

Herein, we report, for the first time, the synthesis of a stable, high-silica zeolite with a PKU-14 structure (named NUD-19) using computationally designed 1-methyl-1-(4-hydroxycyclohexyl)-piperidin-1-ium (SDA1) or 1-ethyl-1-(4-hydroxycyclohexyl)-piperidin-1-ium (SDA2) as the SDA. The two SDAs consist of hydroxyl groups, which could form hydrogen bonds in the gels. Pretreatment of the gel precursor at low temperature facilitates the formation of hydrogen-bonding assemblies of SDAs and significantly regulates the crystallization process, leading to the formation of high-silica and all-silica NUD-19.

2. Experimental section

Synthesis of SDA(OH)

All the chemicals, unless stated otherwise, were purchased without further purification.

The synthesis of the structure-directing agent 1-methyl-1-(4-hydroxycyclohexyl)piperidin-1-ium (SDA1) was performed as follows: a mixture of *trans*-4-aminocyclohexanol (100 mmol, 11.5173 g), potassium carbonate (200 mmol, 26.412 g), and 1,5-dibromopentane (100 mmol, 22.9941 g) was added to a 250 mL round-bottom flask with 200 mL of acetonitrile as the solvent. The reaction was stirred vigorously at 80 °C for 10–12 h. The solvent was then removed by rotary evaporation, and the residue was dissolved in dichloromethane. The solution was filtered to remove the solid, followed by rotary evaporation of the organic solvent to yield a white solid product (yield: 92%–96%). The white solid was redissolved in 200 mL of acetonitrile, and then methyl iodide (400 mmol, 25 mL) was added. The mixture was stirred at 70 °C for 12 h. After removing the solvent by rotary evaporation, a yellow solid was obtained and washed three times with ethyl acetate (3 × 50 mL) to afford the final product (yield: 96%). ^{1}H NMR (400 MHz, DMSO-d$_6$) δ 4.68 (d, J = 4.3 Hz, 1H), 3.52 (tt, J = 11.7, 3.0 Hz, 1H), 3.45–3.33 (m, 5H), 2.85 (s, 3H), 1.97 (dd, J = 53.6, 12.0 Hz, 4H), 1.84–1.68 (m, 4H), 1.40–1.64 (m, 4H), 1.37–1.11 (m, 2H).

SDA2 (Fig. 1) was prepared according to the above procedure by replacing iodomethane with the corresponding bromoethane. ^{1}H NMR (400 MHz, CD$_3$OD) δ 4.78 (s, 1H), 3.68–3.54 (m, 2H), 3.54–3.13 (m, 6H), 2.26–2.02 (m, 4H), 1.95 (ddt, J = 23.3, 11.2, 5.4 Hz, 4H), 1.82–1.58 (m, 4H), 1.53–1.37 (m, 2H), 1.37–1.26 (m, 3H).

The synthesis of the structure-directing agent 1-cyclohexyl-1-methylpiperidin-1-ium (SDA3) was performed as follows: a mixture of cyclohexanamine (100 mmol, 9.92 g), potassium carbonate (200 mmol, 26.412 g), and 1,5-dibromopentane (100 mmol, 22.9941 g) was added to a 250 mL round-bottom
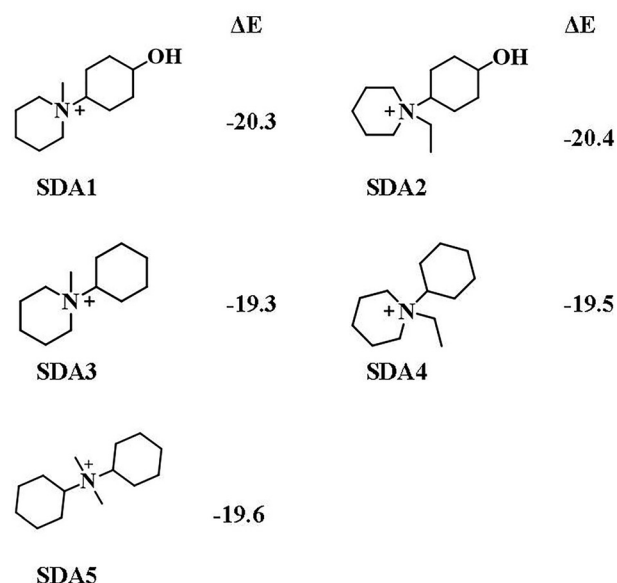

Fig. 1 SDAs and the corresponding calculated interaction energy ΔE (kJ (Si SDA)$^{-1}$) between the SDAs and the siliceous PKU-14 zeolite framework.

flask with 200 mL of acetonitrile as the solvent. The reaction was stirred vigorously at 80 °C for 10–12 h. The solvent was then removed by rotary evaporation, and the residue was dissolved in dichloromethane. The solution was filtered to remove the solid, followed by rotary evaporation of the organic solvent to yield a white solid product (yield: 93%–95%). The white solid was redissolved in 200 mL of acetonitrile, and then methyl iodide (400 mmol, 25 mL) was added. The mixture was stirred at 70 °C for 12 h. After removing the solvent by rotary evaporation, a white solid was obtained and washed three times with ethyl acetate (3 × 50 mL) to afford the final product (yield: 98%). ^{1}H NMR (400 MHz, CD$_3$OD) δ 3.57 (tt, J = 11.6, 3.2 Hz, 1H), 3.53–3.37 (m, 4H), 2.96 (s, 3H), 2.21 (dd, J = 19.6, 9.6 Hz, 2H), 2.03–1.85 (m, 6H), 1.82–1.62 (m, 3H), 1.61–1.37 (m, 4H), 1.32–1.16 (m, 1H).

SDA4 (Fig. 1) was prepared according to the above procedure by replacing iodomethane with the corresponding bromoethane. ^{1}H NMR (400 MHz, CD$_3$OD) δ 3.51–3.33 (m, 5H), 3.30–3.18 (m, 2H), 2.11 (t, J = 18.5 Hz, 2H), 2.00–1.76 (m, 6H), 1.77–1.55 (m, 4H), 1.54–1.33 (m, 2H), 1.31–1.21 (t, 3H), 1.22–1.09 (m, 1H).

For use in zeolite synthesis, the bromide salt of SDA was converted to the corresponding hydroxide solution by ion exchange. The concentration of the hydroxide solution was determined by titration with aqueous hydrochloric acid (0.1000 mol L^{-1}).

Synthesis of germanosilicate NUD-19

In a typical synthesis, 0.1–1.0 mmol of GeO$_2$ were first dissolved in 1.0 mmol of SDA base solution. Then, 1.0 mmol of ethyl orthosilicate was added. The gel was stirred for about two hours at room temperature to ensure complete dissolution.

Then, 1.0 mmol of hydrofluoric acid was added under vigorous stirring. The obtained gel was placed under an infrared lamp or in an oven at 50 °C to remove excess solvent to the theoretical weight according to the final gel molar composition of 1.0 SiO_2 : 1.0 SDA(OH) : 0.1–1.0 GeO_2 : 1.0 HF : 10.0 H_2O. After standing at 0 °C–5 °C for 1–3 days, the gel was transferred to a 15 mL stainless steel reactor with PTFE lining and reacted under sealed conditions at 160 °C for 15 days. The target product was obtained by washing it twice with water and twice with ethanol.

Synthesis of all-silica NUD-19

The all-silica NUD-19 zeolite was synthesized using a seed-assisted strategy with a gel system ratio of 1.0 SiO_2 : 1.0 SDA (OH) : 1.0 HF : 5.0–30.0 H_2O and 1-ethyl-1-(4-hydroxycyclo-hexyl)piperidin-1-ium (SDA2) as the SDA.

In a typical synthesis, 1.0 mmol of SDA(OH) base solution was first mixed with 1.0 mmol of ethyl orthosilicate, and the mixture was magnetically stirred at room temperature for 2 h to ensure complete hydrolysis. Then, 2 wt% of the theoretical gel mass of low-germanium NUD-19 zeolite was added as seeds, followed by the addition of 1.0 mmol of HF solution. The homogeneous gel was obtained by continuous stirring for 30 min. The gel was transferred to a vacuum drying chamber at 50 °C, adjusted to the theoretical gel mass by solvent evaporation, and left at 0 °C–5 °C for 1–3 days to facilitate the colloidal assembly process. The aged gel was loaded into a 15 mL stainless steel reactor with PTFE lining and reacted under sealed conditions at 160 °C for 15 days. The target products were filtered, washed three times each with deionized water and anhydrous ethanol, in turn, and dried at 60 °C for 12 h.

3. Results and discussion

SDAs possessing strong interactions with zeolite frameworks have been shown to be the key for the successful synthesis of some large-pore silica zeolites that were previously available only in high germanium silicate forms.[23] In this study, we computationally designed SDAs with strong interactions with the PKU-14 zeolite framework, targeting the synthesis of pure silica or high-silica PKU-14 zeolites. The germanate zeolite PKU-14 features a unique three-dimensional 12 × 12 × 12-R channel architecture, the corresponding silica or germanosilicate forms of which have not been reported to date. PKU-14 was previously synthesized using *N*-cyclohexyl-*N*,*N*-dimethyl-cyclohexanaminium (SDA5, Fig. 1) as the SDA. We constructed SDAs with similar geometric structures and calculated the interaction energies between the siliceous PKU-14 framework and these SDAs.

SDA1 and SDA2 exhibit larger interaction energies with the PKU-14 framework compared to SDA5, while their analogues SDA3 and SDA4 display smaller interaction energies than SDA5 (Fig. 1). These results indicate that there is a greater likelihood of successfully forming the germanosilicate or silica PKU-14 framework with SDA1 or SDA2 as the SDA. In compari-

son to SDA3 and SDA4, SDA1 and SDA2 each contain an additional hydroxyl group at one end. Upon packing into the channels of the PKU-14 zeolite, the SDA cations align along the three perpendicular straight 12R channels. Calculations revealed that the hydroxyl group of SDA1 or SDA2 forms hydrogen bonds with two neighboring hydroxyl groups inside the 1.18 nm-diameter cavities (Fig. S1 and S2). The formation of hydrogen bonds among SDA1 and SDA2 within the zeolite framework provides additional stabilization energy for the SDA-zeolite assembly, thus facilitating the formation of the zeolite.

Zeolite synthesis with SDA1–SDA4 as SDAs was conducted. Germanosilicate zeolite with the PKU-14 topology (named NUD-19) was successfully synthesized from a gel with a composition of 1 SiO_2 : (0.5–1) SDA(OH) : (0.2–1) GeO_2 : (0.5–1) HF : (3–20) H_2O using either SDA1 or SDA2 as the SDA in the presence of germanium and fluoride ions (Table S1). Moreover, SDA2 demonstrated superior structure-directing capability compared to SDA1, since it directed the formation of NUD-19 with better crystallinity and under wider Si/Ge conditions. In contrast, SDA3 and SDA4 failed to produce PKU-14-type zeolites under similar conditions, and instead formed Beta in the absence of germanium and ITQ-7 or ITQ-17 in the presence of germanium (Table S3). These results are in accordance with the calculations, which show stronger SDA-zeolite interactions of SDA2 than SDA1, and both are stronger than SDA3 and SDA4.

It is noteworthy that the processing conditions for the synthesis gel were related to the crystallization of zeolite NUD-19. NUD-19 was preferably crystallized when the gel precursors were aged at low temperature (*e.g.* 0 °C–5 °C) for a certain period of time before crystallization. The crystallization of NUD-19 with Ge/Si ratios as low as 0.2 could be readily achieved through low-temperature aging of the gels using SDA2 as the SDA. Further experiments demonstrated that the crystallization limitations of pure silica NUD-19 could be overcome by introducing 2 wt% seed crystals into the gel and implementing a low-temperature pretreatment strategy (Fig. S3, S4 and Tables S1, S2). This indicates that the hydroxyl groups on the templating agents could interact with each other and/or gel species to form hydrogen-bonding assemblies under low-temperature aging conditions, thereby enhancing their interactions with the zeolite framework and facilitating the crystallization of NUD-19. This is in accordance with the calculations (Fig. S1 and S2). To verify the effect of low-temperature ageing on the formation of hydrogen bonds, we conducted FT-IR spectroscopic tests on the gels prepared under different conditions. As shown in Fig. S5, the gels prepared under ambient and low-temperature aging show broad strong O–H stretching vibrations at 3395 and 3372 cm^{-1}, respectively, owing to polymeric intermolecular H-bonds between OSDAs. The gel prepared under low-temperature aging has more and stronger H-bonds because of its stronger intensity and lower vibrational frequencies. In contrast, the gel prepared without aging shows weaker and higher O–H stretching vibrations at 3472 cm^{-1}, attributable to single-bridge intramolecular H-bonds.

Powder X-ray diffraction (PXRD) analysis (Fig. 2) revealed that the diffraction peaks of the synthesized products perfectly match the theoretical pattern of PKU-14, confirming that the framework topology of NUD-19 is identical to that of germanate PKU-14. Scanning electron microscope (SEM) and transmission electron microscope (TEM) images showed that NUD-19 consists of well-defined cubic crystals with particle sizes ranging from 30 to 400 nm (Fig. 2 and 3). SDA1–NUD-19 displays lower crystallinity with smaller nanocrystal sizes. The combined results of SEM and PXRD analyses conclusively verify the high phase purity and crystallinity of the NUD-19 product.

The structure determination of NUD-19 proved challenging using conventional single-crystal X-ray diffraction due to its nanoscale crystal dimensions. Consequently, three-dimensional electron diffraction techniques were employed to successfully acquire single-crystal structure data. Continuous rotation electron diffraction (cRED) was utilized for data collection (Fig. 3), with diffraction patterns reconstructed through three-dimensional electron diffraction (3D ED) analysis in reciprocal space. Two-dimensional slices of hkl, $0kl$, and hhl extracted from the 3D ED data are displayed in Fig. 3, enabling precise measurement of cubic system lattice parameters and space group assignments of NUD-19 (synthesized from 1.0 SiO_2 : 1.0 SDA2(OH) : 0.1 GeO_2 : 1.0 HF : 10.0 H_2O).

Structural analysis revealed that NUD-19 crystallizes in the cubic $P432$ space group with unit cell parameters $a = b = c = 13.9350(16)$ Å and a cell volume of $V = 2706.0(9)$ Å^3 (Table S4). The structure of NUD-19 is identical to that of PKU-14. It features a three-dimensional pore system composed of three intersecting 12R channels (Fig. 4a). The free diameters of the three channels are all 8.35 Å × 8.35 Å (Fig. S6). The three intersecting 12R channels run along the a, b, and c axes, respectively, forming spherical supercages with a diameter of
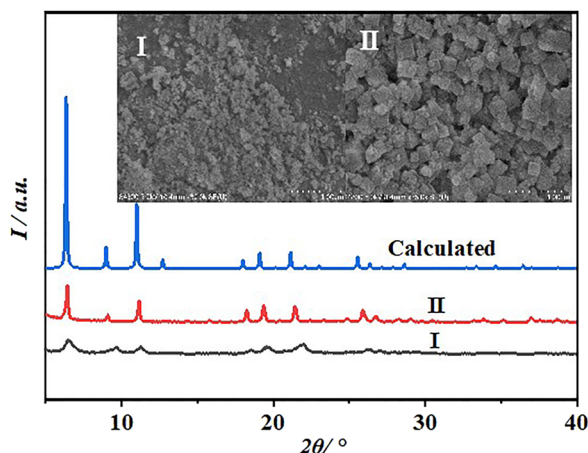

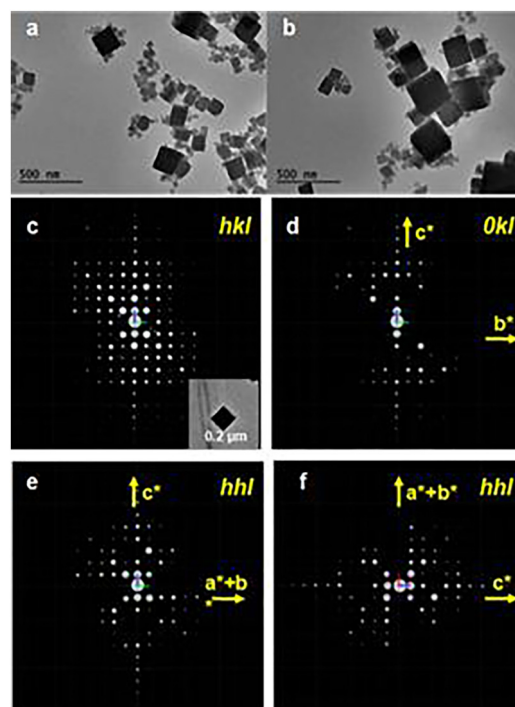**Fig. 3** TEM images (a and b) and 3D crystallographic reconstructions (c–f) of NUD-19.
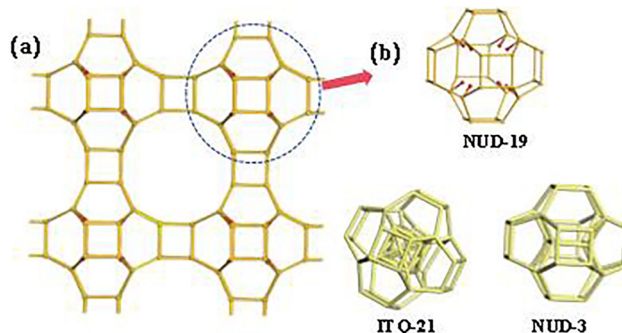
Fig. 4 Crystal structure (a) and structural unit (CBU) image (b) of NUD-19.

Fig. 2 PXRD patterns and SEM images (inset) of (I) the as-made SDA1–NUD-19 (Si/Ge = 2, prepared from 1.0 SiO_2 : 1.0 SDA1(OH) : 0.5 GeO_2 : 1.0 HF : 10.0 H_2O) and (II) as-made SDA2–NUD-19 (Si/Ge = 5, prepared from 1.0 SiO_2 : 1.0 SDA2(OH) : 0.2 GeO_2 : 1.0 HF : 10.0 H_2O), compared with the calculated pattern based on the single crystal structure data.

1.13 nm. From a structural topological perspective, the framework of NUD-19 is constructed from 32-tetrahedra $[4^6 6^{12}]$ composite building units (CBUs), each of which connects six neighboring CBUs *via* its four-membered rings (Fig. 4b). The structure topology of NUD-19 is closely related to that of ITQ-21 and NUD-3, as they are all made of $[4^6 6^{12}]$ cage-like CBUs. The structural distinctions among these materials lie in their CBUs. The cage-like CBUs in ITQ-21 and NUD-3 are both made of 36 tetrahedra, but inside each $[4^6 6^{12}]$ CBU lies a disordered and an ordered T_4O_8 single 4R unit, respectively. In contrast, the CBU of NUD-19 is composed of 32 tetrahedra and empty. That is, inside each CBU, the T_4O_8 single 4R unit present in ITQ-21 and NUD-3 is absent in NUD-19. The missing 4R in the $[4^6 6^{12}]$ CBU results in eight terminal oxygen

or hydroxyl groups pointing toward the center of the cage, giving rise to a spherical void of 4.9 Å in diameter.

The ^{29}Si MAS NMR spectrum of NUD-19 (Si/Ge = 10) is presented in Fig. 5. There are two types of crystallographically-independent Si sites in all-silica NUD-19: one is Q^4 Si(OSi)$_4$ and another is Q^3 (SiO)$_3$Si-OH with an atomic ratio of 3 : 1. The peaks at −109.4 and −115.6 ppm in high-silica NUD-19 are attributed to the Q^4 Si(OT)$_4$ (T = Si and Ge) tetrahedral configurations in NUD-19. The peak at −102.1 ppm originates from the Q^3 (TO)$_3$Si-OH group. The Q^3 sites are mainly due to the absence of the 4R unit inside the [$4^6 6^{12}$] CBU cage, *i.e.*, crystal structural-terminal hydroxyl Si groups on the CBU cage. FT-IR spectroscopy (Fig. S7) revealed that the NUD-19 (Si/Ge = 10) sample dried at 160 °C showed the Si-OH vibration (960–980 cm^{-1}), while no Si-OH vibration was found in the calcined NUD-19. The ^{19}F MAS NMR spectrum of NUD-19 (Fig. S8) showed a strong resonance band at −8.3 ppm, which is due to the fluoride ion being encapsulated in the double-4-member-ring (D4R) unit.[24,25] In addition, the peaks at −122.8 ppm and −128.1 ppm may represent mobile fluoride ions in the channel, which serve as charge balances for SDA cations.

The chemical stability of organic SDAs plays a pivotal role in framework assembly during zeolite synthesis, as the structural integrity of these molecules directly governs crystal nucleation and directional pore channel organization. ^{13}C solid-state NMR spectroscopy (Fig. S9) demonstrates that the ^{13}C chemical shift signatures of SDA2-NUD-19 (synthesized from 1.0 SiO$_2$: 1.0 SDA2(OH) : 0.1 GeO$_2$: 1.0 HF : 10.0 H$_2$O) in the solid state exhibit complete consistency with those of the SDA2 cation in the liquid phase. This observation provides conclusive experimental evidence that no chemical bond cleavage occurred in the SDA2 cation throughout the multi-day crystallization process. Such structural preservation of the SDA critically enables the targeted synthesis of zeolites with specific topological architectures.

The thermogravimetric (TG) profile of NUD-19 (synthesized from 1.0 SiO$_2$: 1.0 SDA2(OH) : 0.1 GeO$_2$: 1.0 HF : 10.0 H$_2$O) under a flow of air exhibits two distinct mass loss steps

Fig. 5 ^{29}Si solid-state MAS NMR spectra of NUD-19.

(Fig. S10). The first step (4.4% mass loss between 70 and 220 °C) corresponds to the loss of physisorbed water molecules. A second prominent weight reduction of 23.5% occurs between 220 and 600 °C, which is attributable to the combustion removal of organic SDAs and fluorine ions trapped within the framework channels. Based on the TG analysis, ICP (Si/Ge = 4.95) and crystal structure of NUD-19, the formula of [Ge$_{5.4}$Si$_{26.6}$O$_{60}$(OH)$_8$]|(C$_{13}$H$_{26}$NOF)$_3$(H$_2$O)$_{7.4}$ is deduced.

NUD-19 exhibits thermal behavior similar to that of all-germanate PKU-14, which showed a 1.7% initial loss of water and a second mass loss of 16.6% within 260–500 °C for removal of organic SDAs, attributed to two water molecules inside each CBU and three SDA5F per unit cell.[14] The higher weight percentage of water and SDAF in NUD-19 is mainly due to the lower atomic weight of silicon than germanium in PKU-14. The physisorbed water molecules mainly reside within the pores, likely inside the [$4^6 6^{12}$] CBU cage. They can freely pass through the 6R windows of the CBU cage, as confirmed by the TG analysis of the pristine and dehydrated samples (heated at 160 °C for 4–5 h, Fig. S10). As the germanium content of the synthesized germanosilicate NUD-19 decreases, the corresponding weight percent of water in NUD-19 increases (Fig. S11). Specifically, NUD-19 prepared at Si/Ge = 2, 5 and 10 contained 1.7, 3.4, and 4.4 wt% of water, respectively, corresponding to approximately 2.9, 5.7 and 7.4 water molecules per unit cell. In other words, the higher the silicon content in NUD-19, the greater the amount of water absorbed, highlighting the superior water adsorption capacity of high-silica NUD-19 compared to its germanate counterpart. The increased water adsorption capacity of NUD-19 with higher Si content could be attributed to the presence of an increased amount of more polar terminal hydroxyl Si groups.

To evaluate the stability of NUD-19 (Si/Ge = 0.2), the organic template agents and residual HF within the channels were removed *via* calcination at 550 °C under air for 6 h. As shown in Fig. S12, high-silica NUD-19 not only retained its characteristic diffraction peak positions after high-temperature treatment, but also demonstrated an improved crystallinity (*i.e.* increased peak intensities) compared to its pristine state. In addition, NUD-19 remained structurally stable when treated in aqueous solution at 120 °C for more than 16 h (Fig. S13). These results confirm that the synthesized NUD-19 possesses exceptional structural integrity and thermal stability. In contrast, the all-germanate PKU-14 zeolite exhibits very limited thermal stability due to its weak Ge–O bonds, with its framework undergoing distortion and collapse at temperatures as low as 350 °C.

Analysis of N$_2$ adsorption–desorption isotherms of calcined NUD-19 (Si/Ge = 10) revealed two distinct features (Fig. 6): (1) a sharp N$_2$ uptake at low relative pressures (0 < P/P_0 < 0.01), indicative of microporosity, and (2) a hysteresis loop at high relative pressures (0.6 < P/P_0 < 1), confirming the presence of mesopores. The latter likely results from the agglomeration of nanoparticles of NUD-19. The pore size distribution profile demonstrates the coexistence of mesopores and micropores. Compared to the all-germanate PKU-14, NUD-19 exhibits a higher Brunner–Emmett–Teller (BET) surface area (504 m^2 g^{-1} *vs.*

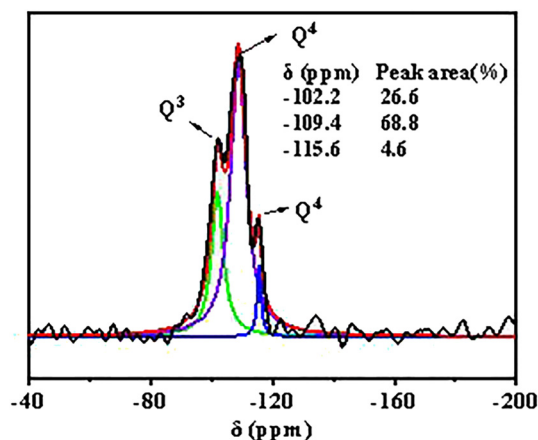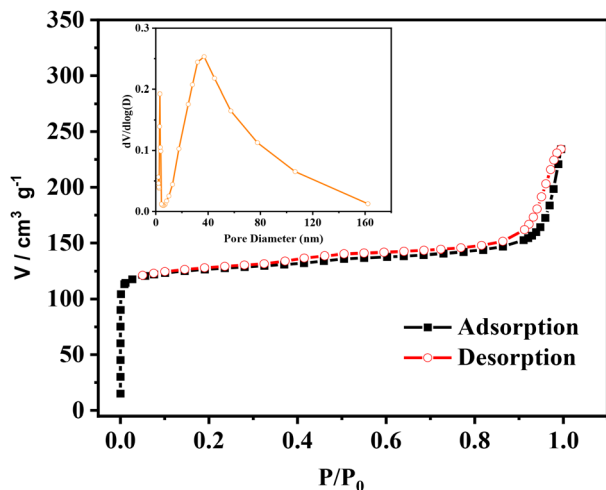**Fig. 6** N₂ adsorption and desorption isotherms (a) and pore size distribution curve (b) of NUD-19 (Si/Ge = 10).

347 m^2 g^{-1}), owing to the lighter formula weight of silica. Notably, NUD-19 possesses a micropore volume of 0.160 m^3 g^{-1}, accounting for 44.2% of the total pore volume (0.362 m^3 g^{-1}, Table S6). The mesopore volume of NUD-19 is dominated by 2–50 nm-sized pores, which account for 39.7% of the total pore volume (Table S6). Collectively, these findings establish NUD-19 as a nanoscale, three-dimensional large-pore hierarchical zeolite.

Conclusions

In summary, we reported a new strategy that utilizes hydrogen-bonding assemblies of organic cations as SDAs to synthesize a three-dimensionally interconnected large-pore high-silica zeolite NUD-19, which is isostructural to all-germanate PKU-14. The organic cations consisting of hydroxyl groups form hydrogen-bonding assemblies in the gel during the aging stage at low temperature and direct the formation of high-silica and all-silica NUD-19. This strategy offers a pathway for synthesizing the large-pore NUD-19 zeolite that is difficult to produce under conventional conditions, and could be applicable to the synthesis of other new zeolites.

Author contributions

H. Li contributed to the synthesis, analyses and writing of the manuscript. Z. H. Zhang contributed to the structure solution. Y. N. Xu, S. Y. Zhang, P. L. Gu, Q. Hu, Y. Zhang, W. K. Wang and Z. Shi contributed to the data analysis. J. Li and H. B. Du administrated the work, carried out theoretical calculations, and wrote the manuscript.

Conflicts of interest

There are no conflicts to declare.

Data availability

The data supporting this article have been included as part of the SI: figures for PXRD, SEM, TGA, NMR, and structure. Tables for elemental analyses, adsorption and single crystallographic data. See DOI: **https://doi.org/10.1039/d5dt01631b**.

CCDC 2430239 contains the supplementary crystallographic data for this paper.[26]

Acknowledgements

References

1 G. T. Kerr, Hydrothermal Chemistry of Zeolites, *Clays Clay Miner.*, 1983, **31**, 319–320.

2 C. S. Cundy and P. A. Cox, The hydrothermal synthesis of zeolites: history and development from the earliest days to the present time, *Chem. Rev.*, 2003, **103**, 663–702.

3 C. A. Fyfe, H. Strobl, G. T. Kokotailo, C. T. Pasztor, G. E. Barlow and S. Bradley, Correlations between lattice structures of zeolites and their ^{29}Si MAS nmr spectra: zeolites KZ-2, ZSM-12, and Beta, *Zeolites*, 1988, **8**, 132–136.

4 R. M. Barrer, Zeolites and their synthesis, *Zeolites*, 1981, **1**, 130–140.

5 Z. Wang, J. Yu and R. Xu, Needs and trends in rational synthesis of zeolitic materials, *Chem. Soc. Rev.*, 2012, **41**, 1729–1741.

6 Ch. Baerlocher, D. Brouwer, B. Marler and L. B. McCusker, *Database of Zeolite Structures*, **https://www.iza-structure.org/databases** (May. 2025 assessed).

7 Y. G. Bushuev and G. Sastre, Atomistic simulations of structural defects and water occluded in SSZ-74 zeolite, *J. Phys. Chem. C*, 2009, **113**, 10877–10886.

8 V. Tazzoli, M. C. Domeneghetti, F. Mazzi and E. Cannillo, The crystal structure of chiavennite, *Eur. J. Mineral.*, 1995, **7**, 1339–1344.

9 M. Estermann, L. McCusker, C. Baerlocher, A. Merrouche and H. Kessler, A synthetic gallophosphate molecular sieve with a 20-tetrahedral-atom pore opening, *Nature*, 1991, **352**, 320–323.

10 T. Willhammar, A. W. Burton, Y. Yun, J. Sun, M. Afeworki, K. G. Strohmaier, H. Vroman and X. Zou, EMM-23: a stable high-silica multidimensional zeolite with extra-large trilobe-shaped channels, *J. Am. Chem. Soc.*, 2014, **136**, 13570–13573.

11 F. Gramm, C. Baerlocher, L. B. McCusker, S. J. Warrender, P. A. Wright, B. Han, S. B. Hong, Z. Liu, T. Ohsuna and O. Terasaki, Complex zeolite structure solved by combining powder diffraction and electron microscopy, *Nature*, 2006, **444**, 79–81.

12 L. A. Villaescusa, J. Li, Z. Gao, J. Sun and M. A. Camblor, IDM–1: A zeolite with intersecting medium and extra–large pores built as an expansion of zeolite MFI, *Angew. Chem., Int. Ed.*, 2020, **59**, 11283–11286.

13 A. Corma, M. J. Díaz-Cabañas, J. Martínez-Triguero, F. Rey and J. Rius, A large-cavity zeolite with wide pore windows and potential as an oil refining catalyst, *Nature*, 2002, **418**, 514–517.

14 J. Liang, J. Su, Y. Wang, Y. Chen, X. Zou, F. Liao, J. Lin and J. Sun, A 3D 12-Ring Zeolite with Ordered 4-Ring Vacancies Occupied by $(H_2O)_2$ Dimers, *Chem. – Eur. J.*, 2014, **20**, 16097–16101.

15 F.-J. Chen, Z. R. Gao, J. Li, L. Gómez-Hortigüela, C. Lin, L. Xu, H.-B. Du, C. Márquez-Álvarez, J. Sun and M. A. Camblor, Structure–direction towards the new large pore zeolite NUD-3, *Chem. Commun.*, 2021, **57**, 191–194.

16 *Insights into the chemistry of organic structure-directing agents in the synthesis of zeolitic materials, Structure and Bonding 175*, ed. L. G. Hortigüela, Springer, 2018.

17 X. Cai, Y. Zhao, J. Zhang, W. Zi, S. Tao, F. Jiao and H. Du, Direct synthesis of an aluminosilicate pos zeolite with intersecting 12× 11× 11−member–ring pore channels by using a designed organic structure–directing, *Chem. – Eur. J.*, 2022, **28**, e202201075.

18 C. Lei, Z. Dong, C. Martínez, J. Martínez-Triguero, W. Chen, Q. Wu, X. Meng, A. N. Parvulescu, T. De Baerdemaeker and U. Müller, A cationic oligomer as an organic template for direct synthesis of aluminosilicate ITH zeolite, *Angew. Chem.*, 2020, **132**, 15779–15785.

19 F. Jiao, J. Zhang, X. Cai, H. Li, Y. Xu, Y. Zhao and H. Du, A fluoride-free siliceous STW-type zeolite synthesized using a designed organic structure-directing agent, *Chem. Commun.*, 2023, **59**, 1649–1652.

20 A. Corma, F. Rey, J. Rius, M. J. Sabater and S. Valencia, Supramolecular self-assembled molecules as organic directing agent for synthesis of zeolites, *Nature*, 2004, **431**, 287–290.

21 W. W. Zi, Z. Gao, J. Zhang, B. X. Zhao, X. S. Cai, H. B. Du and F. J. Chen, An extra–large–pore pure silica zeolite with 16× 8× 8−membered ring pore channels synthesized using an aromatic organic directing agent, *Angew. Chem., Int. Ed.*, 2020, **59**, 3948–3951.

22 F. J. Chen, Y. Xu and H. B. Du, An extra–large–pore zeolite with intersecting 18−, 12−, and 10−membered ring channels, *Angew. Chem. Int. Ed.*, 2014, **53**, 9592–9596.

23 H. Luan, Q. Wu, J. Wu, X. Meng and F.-S. Xiao, Templates for Synthesis of zeolites, *Chin. J. Struct. Chem.*, 2024, **43**, 100252.

24 R. T. Rigo, S. R. G. Balestra, S. Hamad, R. Bueno-Perez, A. R. Ruiz-Salvador, S. Calero and M. A. Camblor, The Si–Ge substitutional series in the chiral STW zeolite structure type, *J. Mater. Chem. A*, 2018, **6**, 15110–15122.

25 I. Saha, A. Erlebach, P. Nachtigall, C. J. Heard and L. Grajciar, Germanium distributions in zeolites derived from neural network potentials, *Catal. Sci. Technol.*, 2024, **14**, 5838–5853.

26 H. Li, Z. Zhang, Y. Xu, S. Zhang, P. Gu, Q. Hu, Y. Zhang, W. Wang, Z. Shi, X. Fu, J. Li and H. Du, CCDC 2430239 NUD-19: Experimental Crystal Structure Determination, 2025, DOI: **10.5517/ccdc.csd.cc2mkvtw**.